doi:10.3772/j.issn.1006-6748.2018.04.012

PMSM speed control using adaptive sliding mode control based on an extended state observer①

Liu Jing(刘 京)[*,**], Xia Peipei②[*,**], Deng Yongting[*], Li Hongwen[*], Wang Zhiqian[*]
([*] Changchun Institute of Optics, Fine Mechanics and Physics, Chinese Academy of Sciences, Changchun 130033, P. R. China)
([**] University of Chinese Academy of Sciences, Beijing 100049, P. R. China)

Abstract

In this study, a composite strategy based on sliding-mode control (SMC) is employed in a permanent-magnet synchronous motor vector control system to improve the system robustness performance against parameter variations and load disturbances. To handle the intrinsic chattering of SMC, an adaptive law and an extended state observer (ESO) are utilized in the speed SMC controller design. The adaptive law is used to estimate the internal parameter variations and compensate for the disturbances caused by model uncertainty. In addition, the ESO is introduced to estimate the load disturbance in real time. The estimated value is used as a feed-forward compensator for the speed adaptive sliding-mode controller to further increase the system's ability to resist disturbances. The proposed composite method, which combines adaptive SMC (ASMC) and ESO, is compared with PI control and ASMC. Both the simulation and experimental results demonstrate that the proposed method alleviates the chattering of SMC systems and improves the dynamic response and robustness of the speed control system against disturbances.

Key words: permanent-magnet synchronous motor (PMSM), adaptive sliding-mode control, extended state observer, speed control

0 Introduction

With the development of power electronics, microprocessors and digital signal processors, the permanent-magnet synchronous motor (PMSM), which has the characteristics of high efficiency, high power density, high torque to inertia ratio, high reliability and easy maintenance, is now used extensively in various industrial applications (e. g., robots, optoelectronic turntables, aerospace applications, and numerically controlled machine tools) that require high-precision control of the motor.

It is well known that a vector control speed-adjustable system of a PMSM usually adopts a proportional integral (PI) controller. However, the PMSM is a nonlinear, multivariable, strongly coupled, and variable parameter system that is extremely sensitive to parameters and disturbance. A PI controller, which is not adaptive to variable parameters and handles disturbances poorly, cannot meet the high-precision control requirements of PMSM.

Recently, with the rapid development of the modern control theories, many researchers have contributed to the design of nonlinear control methods for the PMSM, e. g., adaptive control[1,2], robust control[3,4], intelligent control[5,6], model predictive control[7], and sliding-mode control[8,9]. Among the above methods, sliding-mode control (SMC) method is well known for its advantages such as simple implementation, strong robustness, and quick response, which can provide high performance despite model uncertainties.

So far, SMC has been successfully used in a few PMSM control systems, but with respect to controlling performance, some problems exist. Ref. [10] suggested that SMC could be made more robust to disturbances by increasing the switching gain, however, this aggravates the inherent chattering of SMC, which substantially reduced the system control performance.

To sovle the trade-off between sliding-mode chattering and robustness performance, an adaptive method that observes disturbances and estimates parameters to decrease the amplitude of the switching can be adopted. This approach improves the anti-disturbance performance of the SMC system while attenuating the chattering. In Ref. [11], an SMC method with an adaptive

① Supported by the National Natural Science Foundation of China (No. 11603024).
② To whom correspondence should be addressed. E-mail: peiwaer07@163.com
Received on Nov. 15, 2017

control was developed, which reduced the disturbances caused by parameter uncertainty, and thus improved system dynamic response and attained high static accuracy. In Ref. [12], an SMC method with an extended state observer was proposed. In this approach, the load disturbance was observed by extended state observer (ESO) and the observed value was then applied to the output side of the controller as feed-forward compensation, which enhanced system robustness under load disturbance and effectively alleviated system chattering. An ESO is a high performance observer, which can obtain not only the state of uncertain objects, but also the real-time control quantity of the internal and external disturbances in the object model. The control quantity is compensated for in the control system, achieving a good control result.

Motivated by the above approach, and taking into consideration the influence of parameter variations and load disturbance on the performance of a speed servo system in a PMSM, this paper develops an SMC approach for systems with parameter variations and external disturbance via an adaptive law and ESO. By designing an adaptive law, the system can estimate the internal parameter variations and compensate for the disturbance caused by the model uncertainty. And then, an ESO is designed to estimate the external load disturbance in real time, subsequently, the estimated value is applied as a feed-forward signal to compensate for the speed adaptive SMC (ASMC) controller. There are mainly two remarkable features of the proposed method. First, ASMC deals with the system parameter variations to ensure the global asymptotic stability and to speed up the system response. Second, the high-frequency switching gain in the proposed control law is only required to be designed greater than the bound of the disturbance estimation error rather than that of the disturbance, which alleviates the chattering problem substantially and thus increases the robustness of the system to disturbances.

This paper is organized as follows. In Section 1, a mathematical model of PMSM is described. Section 2 explains the control strategy of an ESO via ASMC, where the convergence of the output tracking error is proven using Lyapunov stability theory. In Section 3, the results of a simulation and experiment are presented to demonstrate the effectiveness of the proposed control scheme. In Section 4, the paper is concluded.

1 Mathematical model of PMSM

For simplicity, in the following analysis, unsaturated PMSM iron core is assumed, the space magnetic field is a sinusoidal distribution, and the hysteresis power losses and eddy current losses are negligible.

Taking the rotor coordinates (d-q axis) of the motor as reference coordinates, the voltage equations can be expressed as

$$\begin{cases} u_d = R_s i_d - \omega L_q i_q + L_d \dfrac{\mathrm{d}i_d}{\mathrm{d}t} \\ u_q = R_s i_q + \omega L_d i_d + \omega \psi_a + L_q \dfrac{\mathrm{d}i_q}{\mathrm{d}t} \end{cases} \tag{1}$$

where, u_d and u_q are the direct axis and quadrature axis stator voltages, R_s is the stator resistance of motor, i_d and i_q are the direct axis and quadrature axis stator currents, ω is the mechanical angular speed of the rotor, $L_q = L_d = L$ are the stator inductances for the PMSM, and ψ_a denotes the flux linkages of the permanent magnet rotor.

The electromagnetic torque equation can be expressed by

$$T_e = \frac{3}{2} p[\psi_a i_q + (L_d - L_q) i_d i_q]$$

where, T_e is electromagnetic torque developed by the motor and p is the number of pole pairs.

Using a field-oriented PMSM control approach, direct axis current i_d is maintained at zero to maximize the output torque. Thus, the electromagnetic torque equation can be rewritten as

$$T_e = \frac{3}{2} p \psi_f i_q = K_t i_q \tag{2}$$

where K_t is the torque constant.

The mechanical equation can be expressed as

$$J \frac{\mathrm{d}\omega}{\mathrm{d}t} = T_e - B\omega - T_l \tag{3}$$

where, J is the moment of inertia, T_l is the external load torque, and B is the viscous friction coefficient.

In the PMSM speed servo system, PI control methods are employed in the two current loops. The system is constructed by composite speed control method, which is straightforward combination of ASMC with the ESO-based feed-forward compensation. The composite method is proposed to ensure the PMSM control system achieves a preferable control performance in the presence of parameter variations and load disturbances.

2 Control strategy

2.1 ASMC design

The parameter variations of the system are defined as

$$\begin{cases} a' = a + \Delta a \\ b' = b + \Delta b \\ c' = c + \Delta c \end{cases} \tag{4}$$

where, $a = \frac{B}{J}$, $b = \frac{K_t}{J}$, $c = \frac{1}{J}$ are the nominal parameters, $\Delta a = \Delta \frac{B}{J}$, $\Delta b = \Delta \frac{K_t}{J}$, $\Delta c = \Delta \frac{1}{J}$ denote the parameter variations introduced by system parameters of a', b', c' respectively. The dynamic system in Eq. (3) is substituted as follows.

$$\dot{\omega} = -a'\omega + b'i_q - c'T_l \tag{5}$$

It is well known that parameter variations lead to the existence of model uncertainties of the system. It is assumed that the perturbation is bounded, that is, $|\Delta a| \leqslant a_1$, $|\Delta b| \leqslant b_1$, and $|\Delta c| \leqslant c_1$. Model uncertainties can be constructed as follows.

$$f = -a_1\omega + b_1 i_q - c_1 T_l \tag{6}$$

Substituting Eq. (6) into Eq. (5), it can be given:

$$\dot{\omega} = -\frac{B}{J}\omega + \frac{K_t}{J}i_q - \frac{1}{J}T_l + f \tag{7}$$

In the speed control system, the state variable is defined as the speed tracking error e_ω:

$$e_\omega = \omega_{ref} - \omega \tag{8}$$

where ω_{ref} is the given reference speed.

Differentiating the error equation in Eq. (8), it can be rearranged:

$$\dot{e}_\omega = -\frac{B}{J}e_\omega - \frac{K_t}{J}i_q + D - f \tag{9}$$

where $D = T_l/J + B\omega_{\mathrm{ref}}/J$ represents the disturbance terms.

Integral-type sliding-mode surface is introduced as a solution for counteracting the parameter variations and eliminate the steady-state error[13]. The integral-type sliding-mode surface without the differentiation of e_ω, improves the stability of the system[14] and it is defined as follows:

$$s = e_\omega + c_1\int_0^t e_\omega(\tau)\,\mathrm{d}\tau \tag{10}$$

where $c_1 > 0$ is the integral coefficient of the sliding-mode surface.

Once an appropriate control law is applied, then the sliding mode will be obtained in finite time. In the sliding mode condition, the error dynamic meets the following function:

$$s = 0,\ \dot{s} = 0 \tag{11}$$

Eq. (11) under the sliding-mode surface in Eq. (10) satisfies:

$$\dot{e}_\omega + c_1 e_\omega = 0 \tag{12}$$

It is clear that in Eq. (12), the value of c_1 decides the decay rate of the speed tracking error. Hence, the error dynamic in the sliding mode can be stabilized.

An important step in the SMC controller design is to derive a suitable control law that satisfies the following sliding-mode accessibility condition.

$$s\dot{s} < 0 \tag{13}$$

If the sliding-mode accessibility condition is guaranteed, s will approach zero in a finite time.

Taking the derivative of the sliding-mode surface in Eq. (10) yields:

$$\dot{s} = \dot{e}_\omega + c_1 e_\omega \tag{14}$$

According to the sliding variable structure principle, the sliding-mode accessibility condition in Eq. (13) can only ensure that the system state having an initial position located anywhere in the state space, can move and reach on the sliding surface in finite time. It has no restrictions on the state trajectories of movement[15]. And the integral sliding surface always leads to chattering and long settling time characteristic of the control system[16].

To deal with the chattering problem, a variable exponent part[16] is employed in the reaching law, where a time-varying modified factor $\lambda(x)$ is introduced to the switching gain:

$$\lambda(x) = \frac{1}{\sigma + (1 + 0.8/|x| - \sigma)e^{-12\cdot|x|}} \tag{15}$$

where $0 < \sigma < 1$ is the modified factor.

Considering the long settling time, a power part[15] is applied to the reaching law, which can give the system a higher response speed when the system state is far from the sliding mode surface. The power part is designed as

$$\dot{s} = -k|s|^{\alpha}\mathrm{sgn}(s) \tag{16}$$

where, $k > 0$, $1 < \alpha < 2$.

Then, the sliding mode reaching law can be expressed as with respect to the speed tracking error:

$$\dot{s} = -g\mathrm{sgn}(s) = -(k_1\lambda(e_\omega) + k_2|s|^{\alpha})\mathrm{sgn}(s) \tag{17}$$

where k_1 and k_2 are the switching gains.

Modified switching gain $k_1\lambda(e_\omega)$ is always smaller than original k_1 near the sliding mode surface, and the system chattering can be suppressed. $\lambda(e_\omega)$ decays to approach zero with the movement of system state, and it can overcome the disadvantages of the regular exponent reaching law.

Considering D as the disturbance term, a speed controller which is based on SMC combined with the proposed reaching law, is derived from Eqs (9), (16), and (17):

$$i_q^* = \frac{1}{\frac{K_t}{J}}\left(\left(c_1 - \frac{B}{J}\right)e_\omega - f + g\mathrm{sgn}(s)\right) \tag{18}$$

The sign function $\mathrm{sgn}(s)$ in i_q^* gives rise to chattering. In order to obtain a continuous control signal, the discontinuous sign function in the control law in

Eq. (18) can be replaced by a proper continuous smoothing function[15-17] as

$$\mathrm{sgn}_\delta(s) \approx \frac{s}{|s| + \delta} \tag{19}$$

where δ is a positive constant. However, chattering cannot be alleviated effectively if δ is too small; otherwise, the dynamic response of the sliding motion will be worsen. Thus, under different operating conditions, a fixed continuous function with δ may not suppress the chattering phenomenon effectively. Therefore, δ is designed as a function of e_ω:

$$\delta(e_\omega) = \delta_0 + \delta_1 |e_\omega|$$

where δ_0 and δ_1 are positive constants. Then the modified continuous smoothing function is given by

$$M_\delta(s) \approx \frac{s}{|s| + \delta_0 + \delta_1 |e_\omega|} \tag{20}$$

Eq. (18) can be rewritten as

$$i_q^* = \frac{1}{\frac{K_t}{J}}\left(\left(c_1 - \frac{B}{J}\right)e_\omega - f + gM_\delta(s)\right) \tag{21}$$

In real applications, the parameter variations of f in Eq. (21) are unavailable and can be substituted by estimates of $\hat{f}$. Thus, an adaptive law[18] is introduced to estimate the uncertainties caused by parameter variations online. This is employed according to the following update law:

$$\dot{\hat{f}} = -\beta s \tag{22}$$

where, $\beta > 0$ represents the adaptive estimation gain and determines the speed of adaptive estimation.

Because $\hat{f}$ is an approximation of f, the speed controller in Eq. (21) can be reconstructed as

$$i_q^* = \frac{1}{\frac{K_t}{J}}\left(\left(c_1 - \frac{B}{J}\right)e_\omega - \hat{f} + \mathrm{gM}_\delta(\mathrm{s})\right) \tag{23}$$

where, $\hat{f}$ denotes the adaptive estimates of f. The estimation error between the estimated and actual parameter variations is $e_f = f - \dot{\hat{f}}$.

In each sampling period of the speed loop, parameter variations are considered to vary much more slowly than the system state, that is, $\dot{f} \approx 0$.

Since $\dot{f} \approx 0$, the differential equation of e_f can be approximately reduced to $\dot{e}_f = -\dot{\hat{f}}$.

Analysing the stability of the adaptive controller based on

$$V = \frac{1}{2}s^2 + \frac{1}{2}\frac{1}{\beta}e_f^2 \tag{24}$$

Taking the derivative of V in Eq. (24) and substituting Eqs(9), (14), and (23) into Eq. (24), it can be yielded.

$$\begin{aligned}\dot{V} &= s\dot{s} + \frac{1}{\beta}e_f\dot{e}_f = s(\dot{e}_\omega + c_1 e_\omega) + \frac{1}{\beta}e_f(-\dot{\hat{f}}) \\ &= s\left(-\frac{B}{J}e_\omega - \frac{K_t}{J}i_q^* + D - f + c_1 e_\omega\right) + se_f \\ &= s(\hat{f} - gM_\delta(s) + D - f) + se_f \\ &= s(D - gM_\delta(s))\end{aligned} \tag{25}$$

According to Lyapunov stability theory, the sliding mode existence and accessibility condition is expressed as

$$\dot{V} \leqslant 0 \tag{26}$$

Substituting Eq. (25) into Eq. (26), it can be yielded.

$$g > |D| \tag{27}$$

If Eq. (27) is satisfied, the closed loop control system can be globally asymptotically stable. The states will approach the sliding-mode surface and are able to stay on it generally, that is

$$s = e_\omega + c_1\int_0^t e_\omega(\tau)\,\mathrm{d}\tau = 0 \tag{28}$$

In Eq. (28), the tracking error of the system converges to zero exponentially.

2.2 ESO design

From Eq. (27), it can be seen that switching gain g should increase along with the increase in the range of load disturbance to satisfy Eq. (26). However, larger switching gain results in the system chattering more serious. If the disturbance can be compensated in time, then sliding mode existence and accessibility condition can be satisfied with a a small switching gain and the system chattering is alleviated.

The dynamic equation can be described from Eq. (9) as

$$\dot{\omega} = -\frac{B}{J}\omega + \frac{K_t}{J}i_q^* + f - D - \frac{K_t}{J}(i_q^* - i_q) \tag{29}$$

Given Eq. (29) and $f \approx \hat{f}$, then:

$$\dot{\omega} = a(t) + b_0 i_q^* + \hat{f} \tag{30}$$

where, $a(t) = -D - (K_t/J)(i_q^* - i_q) - \frac{B}{J}\omega$ represents the lumped disturbances, including friction, external load disturbances, and tracking error of current i_q. It should be noted that $b_0 = K_t/J$.

Consider ω as the state variable and $a(t)$ as an extended state, it is defined as

$$x_1 = \omega,\ x_2 = a(t) \tag{31}$$

Based on Eq. (31), Eq. (30) can be rearranged into the following state equation:

$$\begin{cases} \dot{x}_1 = \hat{f} + x_2 + b_0 i_q^* \\ \dot{x}_2 = aa(t) \\ y = x_1 \end{cases} \tag{32}$$

where, $aa(t) = \dot{a}(t)$. According to Ref. [19], linear ESO can be constructed for the extended system of Eq. (31) as follows:

$$\begin{cases} e = z_1 - y \\ \dot{z}_1 = z_2 - L_1 e + \hat{f} + b_0 i_q^* \\ \dot{z}_2 = -L_2 e \end{cases} \tag{33}$$

where, $L_1 = 2\omega_0$, $L_2 = \omega_0^2$, $-\omega_0$ describes desired double pole of the ESO, with $\omega_0 > 0$.

As long as the ESO in Eq. (33) is well designed and tuned, $z_1(t)$ and $z_2(t)$ in the observer of Eq. (33) can estimate the state variables $x_1(t)$ and the extended state of $x_2(t)$ in the system of Eq. (32) quickly with high precision.

The block diagram of the ESO-based speed controller for the PMSM servo system is shown in Fig. 1. The output of the ESO is $z_1(t)$ and $z_2(t)$. $z_1(t)$ will track the motor speed $\omega(t)$ and can be used as speed feedback to the speed controller. $z_2(t)$ can estimate the lumped disturbances of the system and make a feed-forward compensation to the speed controller ASMC. The proposed composite method is called ASMC + ESO method.

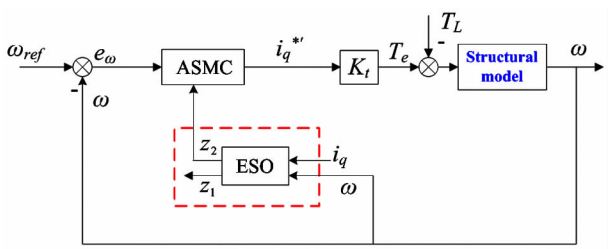

Fig. 1 Schematic diagram of the PMSM speed servo system based on ASMC and ESO

The observed value z_2, makes an equivalent compensation to the speed controller ASMC to reduce switching gain in the control law in Eq. (23). Thus, the speed ASMC law can be obtained with load disturbance feed-forward compensation as

$$i_q^{*'} = \frac{1}{\frac{K_t}{J}}\left(\left(c_1 - \frac{B}{J}\right)e_\omega - \hat{f} + gM_\delta(s) + z_2\right) \tag{34}$$

The term $-\left(\frac{K_t}{J}\right)^{-1} z_2$ is designed to compensate for the item $T_l/J + B\omega/J$ in Eq. (9).

Similarly, according to the Lyapunov stability theory in Eq. (26), the stability condition of the ASMC + ESO method can be derived from Eqs(24) – (26) as follows:

$$\begin{aligned} \dot{V} &= s\dot{s} + \frac{1}{\beta}e_f\dot{e}_f = s(\dot{e}_\omega + c_1 e_\omega) + \frac{1}{\beta}e_f(-\dot{\hat{f}}) \\ &= s\left(-\frac{B}{J}e_\omega - \frac{K_t}{J}i_q^{*'} + D - f + c_1 e_\omega\right) + se_f \\ &= s(\hat{f} - gM_\delta(s) - z_2 + D - f) + se_f \\ &= s(D - gM_\delta(s) - z_2) \end{aligned} \tag{35}$$

$$g > |D - z_2| \tag{36}$$

Comparing Eqs(27) and (36), it is clear that to ensure system stability and robustness, the switching gains of the ASMC and ASMC + ESO methods must be designed as $g > |D|$ and $g > |D - z_2|$, respectively. As the load disturbance can be precisely estimated by ESO, the magnitude of the estimation error $|D - z_2|$ is obviously much smaller than the load disturbance $|D|$. Thus, the ASMC + ESO method can improve the robustness performance of the system further, while alleviating the chattering phenomenon effectively.

3 Simulation and experimental results and discussions

To evaluate the effectiveness of the proposed method, simulations and experiments for the PI, ASMC, and ASMC + ESO methods were carried out. The specifications of the PMSM are shown in Table 1. Simulation was performed on the Matlab/Simulink platform. The experimental platform was constructed using DSP TMS320F28335 and FPGA EP3C40F324 processors. Fig. 2 shows the overall block diagram of the composited speed control method based on ASMC + ESO for the PMSM servo system. The schematic diagram of the experimental platform is shown in Fig. 3.

Table 1 PMSM parameters

Parameters	Value
Armature inductance L	30.08mH
Armature resistance R	15.42 Ω
Torque constant K	0.41Nm · A^{-1}
Number of pole pairs p	4
Rotor inertia J	0.138kg · cm^2

3.1 Simulation settings

The PI simulation parameters of both current loops are the same: proportional gain $k_{pc} = 4.5$, and integral gain $k_{ic} = 0.13$. The PI simulation parameters of the speed loop use proportional gain $k_{p\omega} = 0.012$ and integral gain $k_{i\omega} = 0.002$. The simulation parameters of the ASMC speed loop are $c_1 = 6$, $k_1 = 580$, $k_2 = 130$, α

$= 1.5$, $\sigma = 0.2$, $\delta_0 = 17$, $\delta_1 = 102$, and $\beta = 0.0003$. The simulation parameters of the ASMC + ESO speed loop are $c_1 = 6$, $k_1 = 580$, $k_2 = 130$, $\alpha = 1.5$, $\sigma = 0.2$, $\delta_0 = 17$, $\delta_1 = 102$, $\beta = 0.0003$, and $-\omega_0 = -145$.

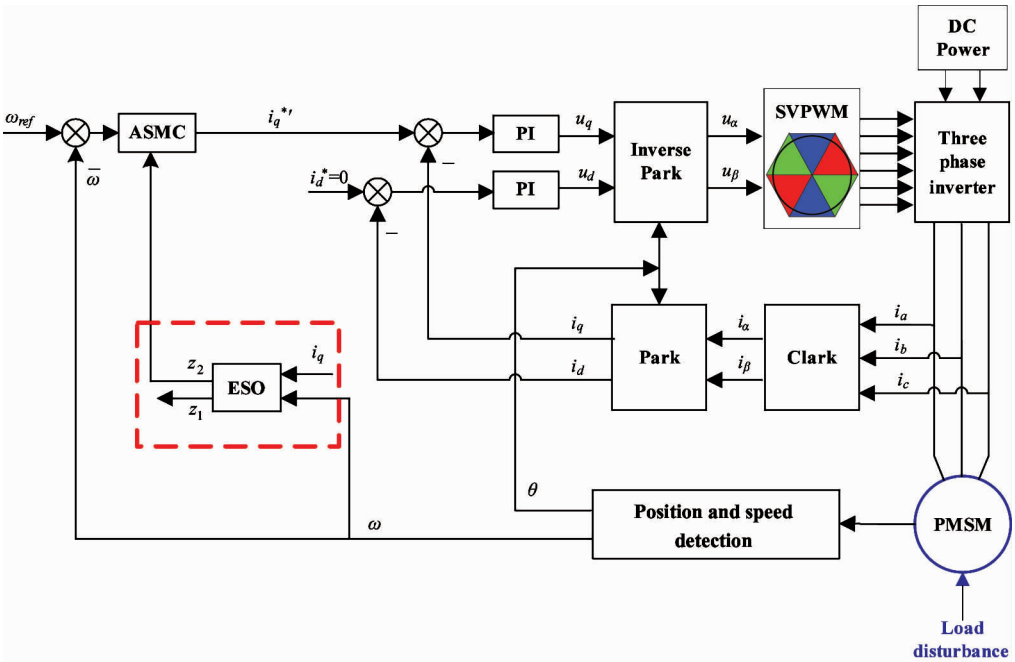

Fig. 2 Schematic diagram of the PMSM speed servo system based on ASMC + ESO

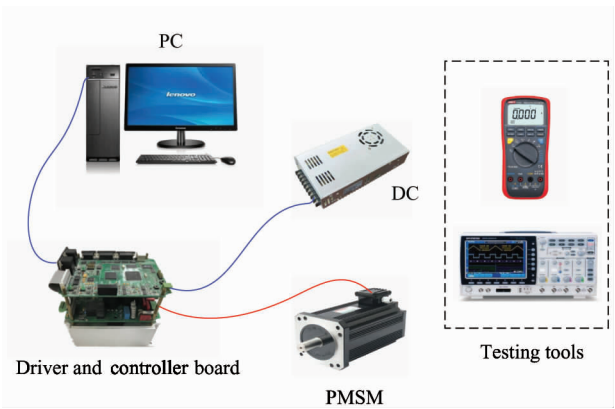

Fig. 3 Schematic diagram of the experimental platform

3.2 Simulation results

The speed command is set to be $-300 \rightarrow +600 \rightarrow -300$ r/min. The simulation results of the speed response and q-axis current response with the three methods are shown in Figs 4 – 6. It can be found that, compared with the speed response of the PI method (13.6% overshoot and 0.02 s settling time), the speed response of the ASMC method has a much smaller overshoot (0%) and a shorter settling time (0.013 s). Moreover, the ASMC + ESO method gives the PMSM speed control system the best dynamic performance (0% overshoot and 0.008 s settling time). Meanwhile, q - axis

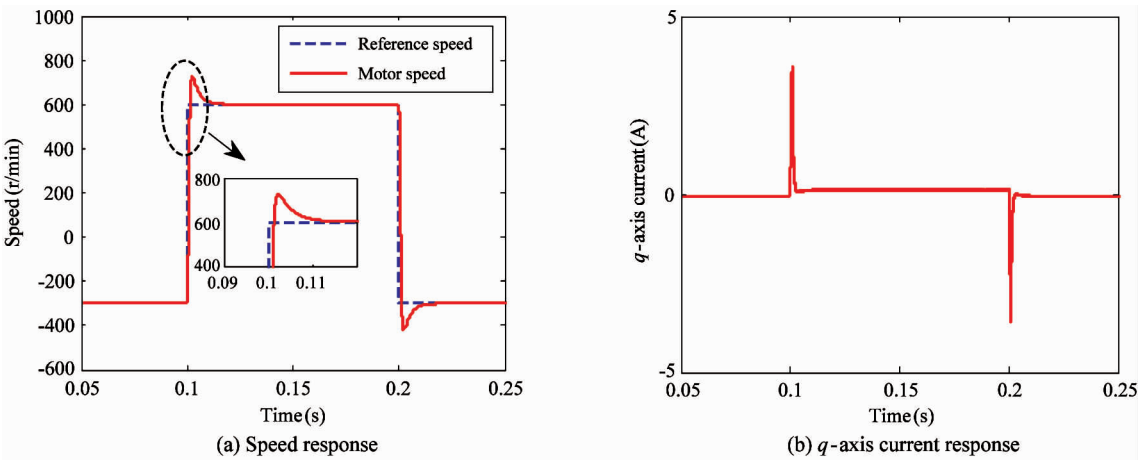

Fig. 4 Simulation results under the PI method

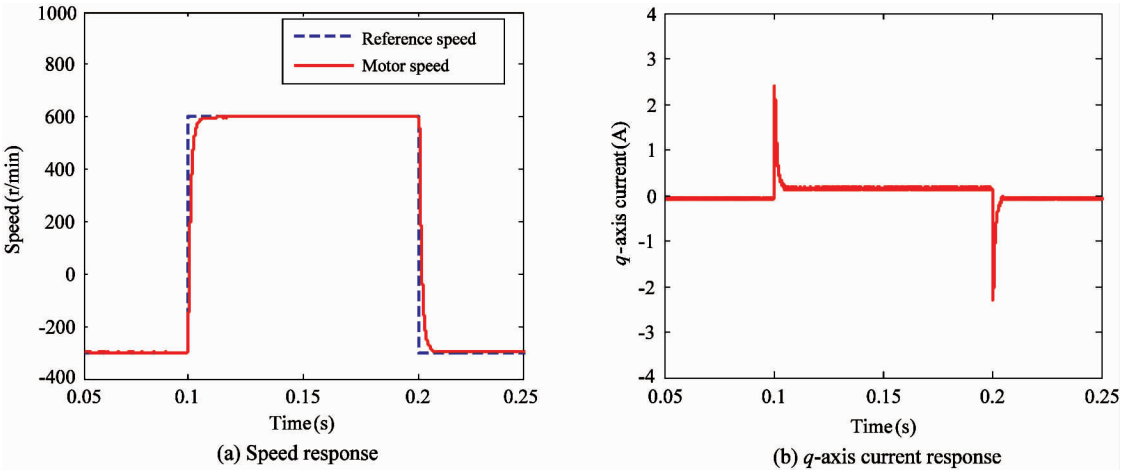

Fig. 5 Simulation results under the ASMC method

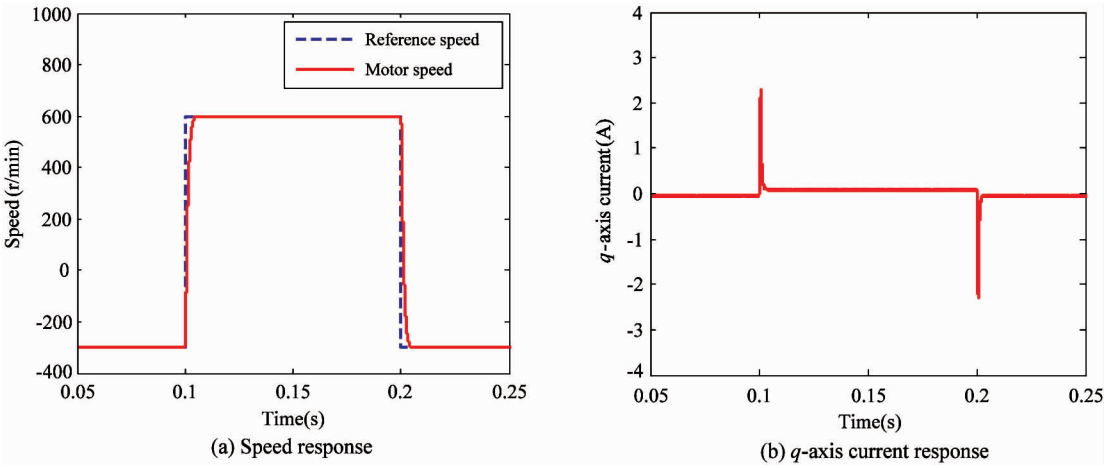

Fig. 6 Simulation results under the ASMC + ESO method

current response has the smallest settling time and overshoot, compared with those of the PI and ASMC methods.

The speed command is set to be 800 r/min, and the load disturbance $T_l = 0.36$ N · m is added abruptly at $t = 0.1$s and removed at $t = 0.2$s. The simulation results of the speed response and q-axis current response with the three methods are shown in Figs 7 – 9. The details of simulation results with respect to the three methods are shown in Table 2.

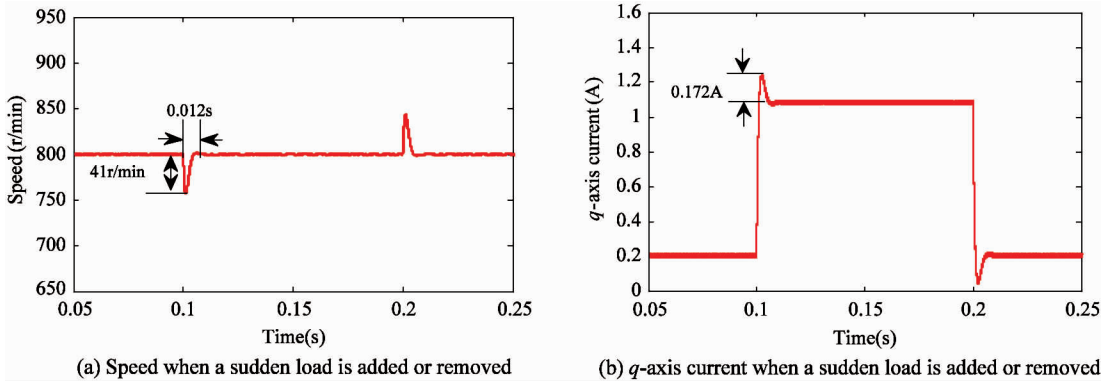

Fig. 7 Simulation results under the PI method

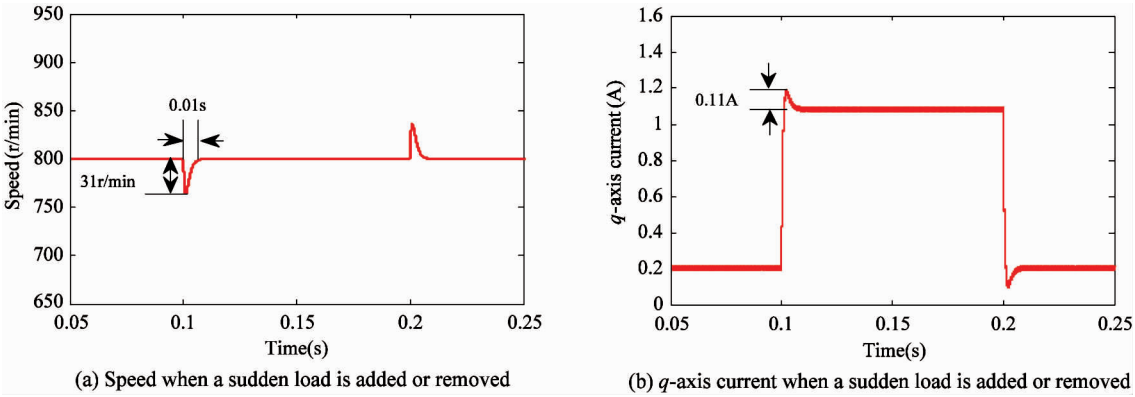

(a) Speed when a sudden load is added or removed (b) q-axis current when a sudden load is added or removed

Fig. 8 Simulation results under the ASMC method

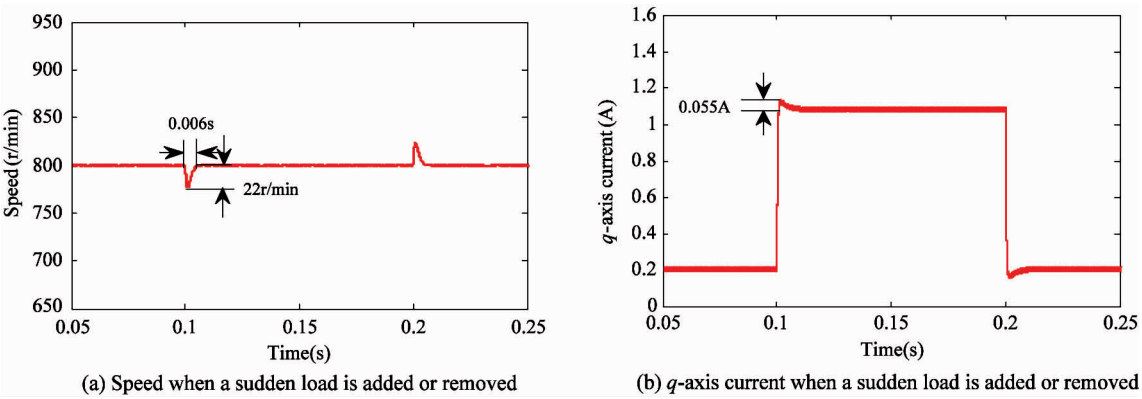

(a) Speed when a sudden load is added or removed (b) q-axis current when a sudden load is added or removed

Fig. 9 Simulation results under the ASMC + ESO method

Table 2 Comparisons of disturbance rejection performance

Control method	PI	ASMC	ASMC + ESO
Speed fluctuation at loading (r/min)	41	31	22
Speed adjustment time at loading(s)	0.012	0.01	0.006
Overshoot in I_q at loading (A)	0.172	0.11	0.055
I_q adjustment time at loading (s)	0.011	0.0092	0.0056

It can be seen that, when the system is in sudden load and unload conditions, the ASMC + ESO method has the least fluctuations in speed and least overshoot of q-axis current. Further, the settling time needed for the speed and q axis current to return to the original value is the smallest. The above results demonstrate that the ASMC + ESO method can obtain more satisfactory system dynamic performance and robustness to disturbances, compared to the PI and ASMC methods. The simulation estimated result of ESO is shown in Fig. 10.

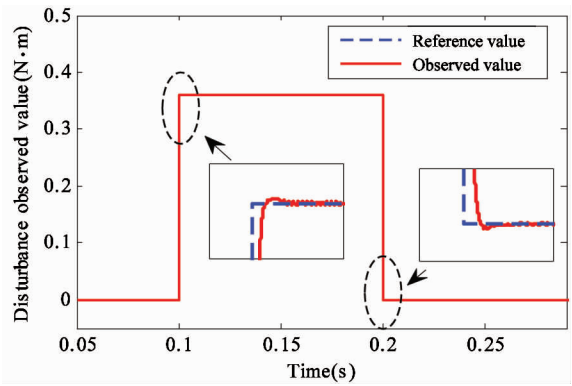

Fig. 10 Estimated results of the ESO (simulation)

3.3 Experiment description

Similar to the simulation, two operating conditions are conducted to evaluate the control performance of the proposed ASMC + ESO method. The hardware configuration of the PMSM speed servo system is shown in Fig. 11. The overall control schematic was built based on the digital signal processor (DSP) and field progrmmable gate array (FPGA). An incremental optical encoder was utilized to measure the digital position and the resolution ratio was 2 500 pulses per revolution (ppr).

A quadruplicated frequency was achieved by FPGA, and the resolution ratio was increased to 10 000 ppr.

The PI parameters of both current loops are the same: proportional gain k_{pc} = 4.8 and integral gain k_{ic} = 0.08. The PI parameters of the speed loop are proportional $k_{p\omega}$ = 0.015 and integral gain $k_{i\omega}$ = 0.002. The parameters of the ASMC speed loop are c_1 = 6, k_1 = 600, k_2 = 120, α = 1.5, σ = 0.2, δ_0 = 16, δ_1 = 90, and β = 0.0003. The parameters of the ASMC + ESO speed loop are: c_1 = 6, k_1 = 600, k_2 = 120, α = 1.5, σ = 0.2, δ_0 = 16, δ_1 = 90, β = 0.0003, and $-\omega_0$ = −110.

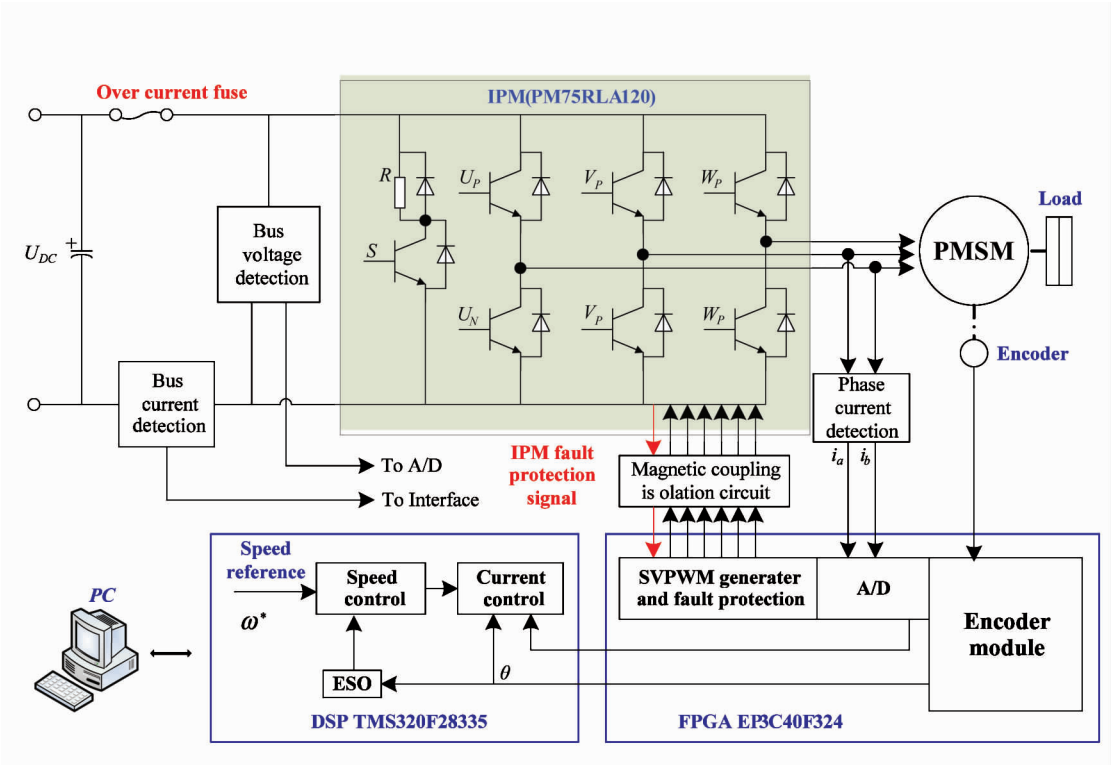

Fig. 11 Hardware configuration of the PMSM drive and control system

3.4 Experimental results

The responses of the speed and current of q axis with the PI, ASMC, and ASMC + ESO methods under a speed command of −300→+600→−300 r/min are shown in Figs 12 − 14. The experimental results clearly show that the ASMC + ESO method achieves a more satisfactory dynamic response than the PI and ASMC methods. The overshoot of the speed response for the PI method is approximately 22%; that for the ASMC and ASMC + ESO methods decreases to approximately zero. The adjustment time for the PI method was approximately 0.5 s, that for the ASMC method decreased to approximately 0.2 s and that for the ASMC + ESO method decreased further to approximately 0.16 s.

Moreover, experiments were carried out under the impact of sudden load and sudden unload disturbances to compare the robustness performance of the PI, ASMC, and ASMC + ESO methods under a speed command of 800 r/min. The load disturbance was realized by the magnetic power brake . The load disturbance torque T_l = 0.36 N · m was added suddenly and removed after a duration of time.

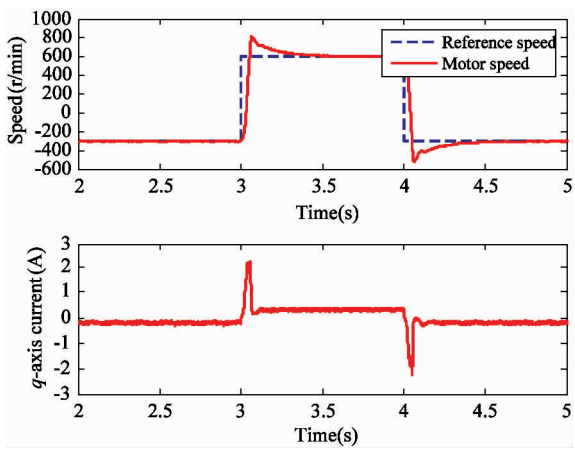

Fig. 12 Experimental results with the speed command of −300→+600→−300 r/min under the PI method: speed response and q axis current response

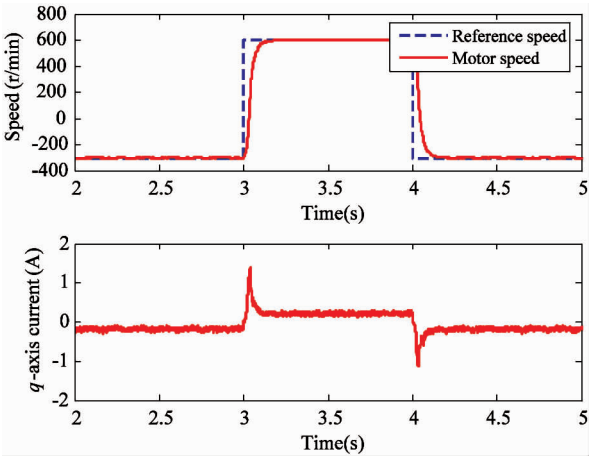

Fig. 13 Experimental results with the speed command of -300 → + 600 →-300 r/min under the ASMC method: speed response and q axis current response

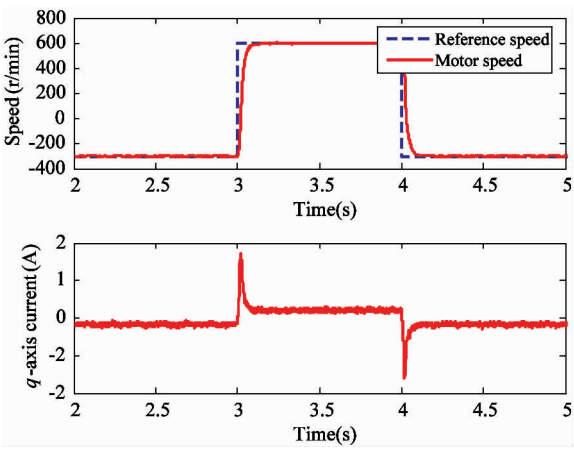

Fig. 14 Experimental results with the speed command of −300 → +600→ −300 r/min under ASMC + ESO method: speed response and q axis current response

The load torque of 0.36 N · m acted as the disturbance on the load side. The dynamic response of the speed and q-axis current are shown in Figs 15 – 17. It is evident that the proposed ASMC + ESO method has a better anti-disturbance capability than the PI and ASMC methods. Compared to the PI and ASMC methods, the ASMC + ESO method gives a smaller fluctuation in speed and a smaller overshoot in q-axis current. In addition, the speed and q-axis current are guaranteed to be restored to their original values much faster. The details of the experimental results are listed in Table 3, which demonstrate that the proposed speed control method enhances the system performance in the presence of load disturbance and alleviates sliding mode chattering effectively.

The experimental results of ESO is shown in Fig. 18. It can be seen that the external load disturbance can be estimated accurately by ESO in real time.

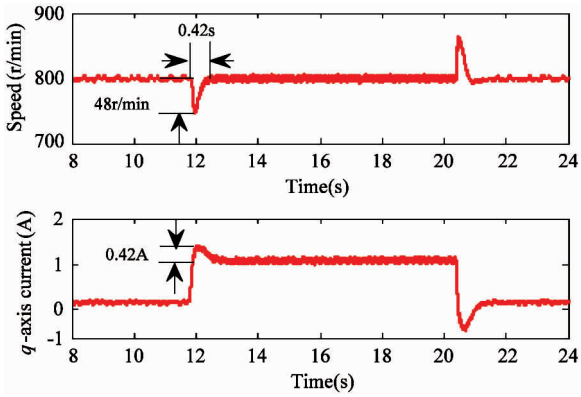

Fig. 15 Experimental results with external disturbance under the PI method: speed response and q-axis current response

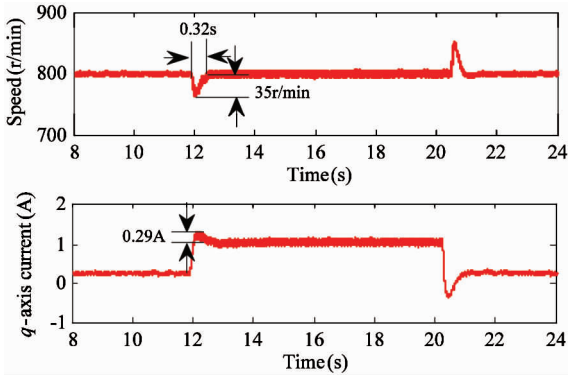

Fig. 16 Experimental results with external disturbance under the ASMC method: speed response and q-axis current response

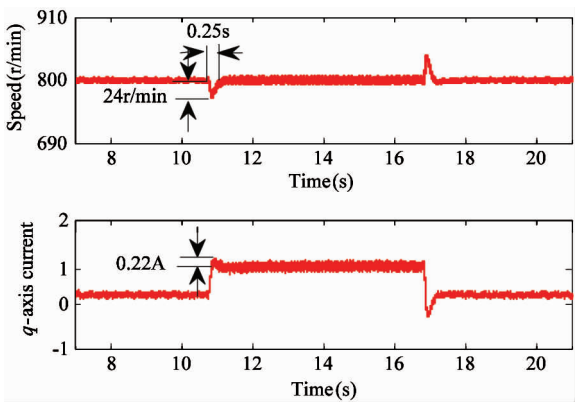

Fig. 17 Experimental results with external disturbance under the ASMC + ESO method: speed response and q-axis current response

The observed value was then used as feed-forward compensation for the ASMC speed controller to improve the robustness of the system.

The simulation and experimental results are consistent with each other. It can be concluded that the ASMC + ESO method improves the dynamic and ro-

bustness performance of PMSM servo system to parameter variations and load disturbance.

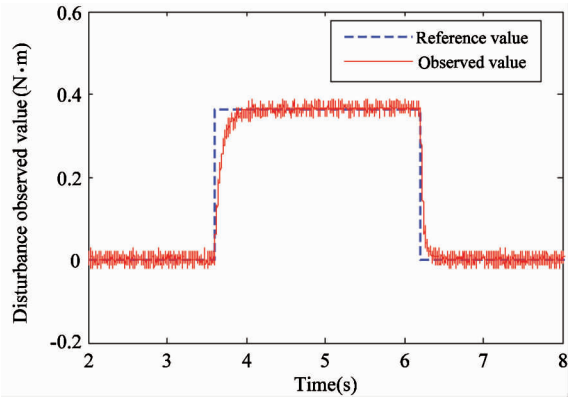

Fig. 18 Estimated results of the ESO (experiment)

Table 3 Comparisons of disturbance rejection performances

Control method	PI	ASMC	ASMC + ESO
Speed fluctuation at loading(r/min)	48	35	24
Speed adjustment time at loading(s)	0.42	0.32	0.25
Overshoot in I_q at loading (A)	0.42	0.29	0.22
I_q adjustment time at loading (s)	0.41	0.3	0.23

4 Conclusion

A composite control strategy ASMC + ESO is presented in this paper. It is employed in a PMSM speed control system, for the purpose of suppression of sliding mode chattering as well as improvement of the anti-disturbance capacity. The major contributions of this study are as follows. 1) An adaptive law was developed to estimate the internal parameter variations and compensate for the disturbance of the model uncertainty. 2) ESO was designed to estimate the load disturbance online, and the estimated value was utilized to compensate the output of the speed ASMC controller. 3) A composite control strategy based on ASMC and ESO was developed to further improve the disturbance robustness of the ASMC system. Both simulation and experimental investigations were conducted to demonstrate the effectiveness and advantages of the proposed composite method. The results indicate that the proposed ASMC + ESO method alleviates system chattering effectively, while enhances the system robustness under parameter variations and load disturbances.

References

[1] Kim S K, Lee K G, Lee K B, et al. Singularity-free adaptive speed tracking control for uncertain permanent magnet synchronous motor[J]. *IEEE Transaction on Power Electronics*, 2016, 31: 1692-1701

[2] Kim S K. Robust adaptive speed regulator with self-tuning law for surfaced-mounted permanent magnet synchronous motor[J]. *Control Engineering Practice*, 2017, 61: 55-71

[3] Ramirez-Villalobos R, Aguilar L T, Coria L N. Sensorless H∞ speed-tracking synthesis for surface-mount permanent magnet synchronous motor[J]. *ISA Transactions*, 2017, 67: 140-150

[4] Jon R, Wang Z S, Luo C M, et al. Adaptive robust speed control based on recurrent elman neural network for sensorless PMSM servo drives[J]. *Neurocomputing*, 2017, 227: 131-141

[5] EL-Sousy F F M. Intelligent mixed H_2/H_∞ adaptive tracking control system design using self-organizing recurrent fuzzy-wavelet-neural-network for uncertain two-axis motion control system[J]. *Applied Soft Computing*, 2016, 41: 22-50

[6] Yu J, Shi P, Dong W, et al. Neural network-based adaptive dynamic surface control for permanent magnet synchronous[J]. *IEEE Transaction Neural Networks and Learning Systems*, 2015, 26(3): 640-645

[7] Tarzewski T, Grzesiak M. Constrained state feedback speed control of PMSM based on model predictive approach[J]. *IEEE Transactions on Industrial Electronics*, 2016, 63(6): 3867-3875

[8] Song Q, Jia C. Robust speed controller designed for permanent magnet synchronous motor drives based on sliding mode control[J]. *ScienceDirect*, 2016, 88: 867-873

[9] Su D D, Dong Y G, Zhang C N. Sliding mode controller for permanent magnetic synchronnous motors[J]. *ScienceDirect*, 2017, 105: 2641-2646

[10] Liu Y, Zhou B, Famg S C. Sliding mode control of PMSM based on a novel disturbance observer[J]. *Proceedings of the CSEE*, 2010, 30(9): 80-85

[11] Chang S H, Chen P Y, Ting Y H, et al. Robust current control-based sliding mode control with simple uncertainties estimation in permanent magnet synchronous motor drive systems[J]. *IET Electric Power Applications*, 2014, 4(6): 441-450

[12] Xia C L, Liu J H. Variable structure control of BLDCM based on extended state observer[J]. *Proceedings of CSEE*, 2006, 26(20): 139-143

[13] Utkin V, Shi J X. Integral sliding mode in systems operating under uncertainty condition[C]. In: Proceedings of the 35th IEEE Conference on Decision and Control, 1996. 4591-4596

[14] Li Z, Hu G D, Cui J R, et al. Sliding-mode variable structure control with integral action for permanent magnet synchronous motor[J]. *Proceeding of the CSEE*, 2014, 34(3): 431-437

[15] Liu J K. Sliding Mode Control Design and MATLAB Simulation[M]. Beijing : Tsinghua University Press, 2012, Chap. 1-2 (In Chinese)

[16] Jin N Z, Wang X D, Wu X G. Current sliding mode control with a load sliding mode observer for permanent magnet synchronous machines[J]. *Jouanal of Power Electronics*, 2014, 14(1): 105-114

[17] Chern T L, Wu Y C. Design of integral variable structure controller and application to electrohydraulic velocity servo systems[J]. *IEE Proceedings-D*, 1991, 138(5): 439-444

[18] Hou L M, Zhang H G, Liu X Y. Adaptive sliding mode controller based on extended observer of SPMSM with active disturbance rejection passivity-based controller[J]. *Control and Decision*, 2010, 25(11): 1625-1656

[19] Gao Z. Scaling and bandwidth parameterization based controller tuning[C]. In: Proceeding of the American Control Conference, 2006. 4989-4996

Liu Jing, born in 1991. She is currently working toward Ph. D degree in the Changchun Institute of Optics, Fine Mechanics and Physics, Chinese Academy of Sciences, Changchun, China, and the University of Chinese Academy of Sciences, China. She received the B. E. degree in electrical engineering from the Nanjing University of Aeronautics and Astronautics, Nanjing, China, in 2013. Her research interests include electric machines and drives and high-precision machine control techniques.